Gas-solid two-phase flow in 90° bend

K.A. Ibrahim, M.A. El-Kadi, Mofreh H. Hamed and Samy M. El-Behery
Faculty of Engineering, Menoufiya University, Shebin El-kom, Egypt

Gas-solid two-phase flows are numerically simulated in a 90° bends The numerical calculations are performed by Eulerian approach for the gas-phase taking into account the mutual effects of the solids on the gas, and Lagrangian approach for the dispersed-phase. Two particulate turbulence models have been studied to predict turbulent gas-solid flows in bends. The first one is based on the standard k-ε model, while the second model is RNG (Renormalization Group) based k-ε model. Comparisons are made with theoretical results and experimental data for the mean axial flow velocities of both phases and these comparisons show a good agreement. The present results help to understand the physical phenomena occurring in gas-solid flows in 90° bends. In addition the results also show that behaviour of gas-solid two-phase flows in bends is affected greatly by inlet gas velocity, particle diameter, curvature ratio and mass loading ratio. The present calculations also reveal that, the total pressure loss for gas-solid two-phase flow in 90° bend is greater than the corresponding value obtained for gas only and its value is greatly affected by the fluid and solid parameters.

تم محاكاة السريان الاضطرابى ثنائي الطور لغاز وجسيمات صلبة خلال قنوات أفقية منحنية بزاوية ٩٠° . تعتمد الدراسة العددية على معادلات أويلر لسريان الغاز الاضطرابى وتأخذ فى الاعتبار تأثير الجسيمات الصلبة على الغاز بينما تستخدم معادلات لجرانج لحركة الجسيمات الصلبة. كما اعتمد النموذج المقترح على ربط معادلات البقاء للغاز والجسيمات مستخدما نموذجين مختلفين الأول منهما هو الموديل القياسى للاضطراب(k-ε) والثانى هو (RNG based k-ε) المعتمد على النموذج القياسى لحساب اضطراب طاقة الحركة ومعادلة التشتت. كما يأخذ النموذج فى الاعتبار اصطدام الجسيمات الصلبة مع أسطح هذه الأنابيب المنحنية وارتدادها. ولفحص دقة هذا النموذج المقترح ودرجة الاعتماد عليه فقد أجريت مقارنة بين تنبؤات النموذجين المقترحين ونتائج عملية سابقة منشورة لآخرين. وقد أظهرت هذه المقارنة توافقا جيدا وأن استخدام النموذج الثانى أفضل. كم أوضحت نتائج هذه الدراسة تأثير كل من سرعة الغاز الابتدائية ، معدل تحميل الجسيمات ، نسبة التقوس ، وكذا قطر الجسيمات على كل من توزيعات السرعة المحورية لكل من الغاز والجسيمات الصلبة والفقد فى الضغط ومعامل الفقد فى الأنابيب المنحنية وكذا على مسار هذه الجسيمات داخل هذه الأنابيب. كما أوضحت الدراسة أهمية النتائج التى تم الحصول عليها لاستخدامها فى فهم سلوك كل من الغاز المضطرب وحركة الجسيمات الصلبة خلال هذه الأنابيب المنحنية.

Keywords: Turbulent flow, Curved duct, Gas-solid, Particle collision, Particle trajectory

1. Introduction

Gas-solid two-phase flows are encountered in a wide range of industrial applications. Bends and elbows are commonly used in many of these applications such as, pneumatic conveyers; coal fired power plants, food processing, chemical industries, pneumatic dryers and moving of dusty gas in heat exchangers. When the gas-solid mixture flows through a bend the solid particles form a ropelike structure because of inertial effects. The particle rope, which carries most of the conveyed material within a small portion of the pipe cross-section, has low particle velocity and high concentration. Gas-solid flow structure through and after bends have been studied numerically and experimentally by many researchers [1-7]. Yilmaz and Levy [1] studied numerically, based on RNG k-ε model, the flow through bend but the effects of particle rotation, shear lift and Magnus lift due to particle rotation on the flow structure especially near the wall were not taken into account. Huber and Sommerfeld [2] investigated numerically, using standard k-ε model, the flow in a bend (R_c/D = 2.54) only at a mass loading ratio of 0.3. Akilli et al. [3] investigated both experimentally and numerically, using standard k-ε model, the effects of flow parameters on the behavior of gas-solid flow in horizontal pipe after a 90° vertical-to-horizontal elbow. Bilirgen and levy [4] investigated both experimentally and numerically the

flow behaviour through bends using standard k-ε model and taking into account the drag force only. Kuan et al. [5] investigated numerically and experimentally the flow behavior in a rectangular horizontal-to-vertical bend at very low solids mass loading ratio. Kuan [6] continued his investigation [5] to study the effect of different size distributions of solids on the flow behaviour. Both [5, 6] neglected the effect of dispersed phase on the gas phase (mutual effects). Hidayat and Rasmuson [7] performed numerical investigation of gas-solid two-phase flow in a U-bend using Eulerian-Eulerian model. It is well known that the standard *k-ε* model failed to simulate the flow subjected to streamline curvature due to the anisotropic structure that formed by the bend. So the use of RNG based *k-ε* model will apparently cover this failer. It appears from the previous discussion that there is a little information exists on using RNG based *k-ε* model for the flow through the bend. Therefore, in the present work the effect of flow parameters on the flow behavior in a horizontal 90° bend are studied numerically using the two aforementioned turbulence models to simulate the gas-solid two-phase flow in bends taking into account the effect of particle rotation, shear lift and Magnus lift due to particle rotation on the flow structure.

2. Mathematical modelling

The numerical calculations is performed using Eulerian approach for gas-phase, taking into account the mutual effects of the solids on the air, and Lagrangian approach for dispersed-phase, considering that all the particles have been introduced in the flow with approximately the same bulk velocity of the fluid. The particulate phase consists of spherical particles.

2.1. Fluid flow modelling

The gas flow calculations are based on the time averaged Navier-Stokes equations in connection with two turbulent models namely standard model and RNG based *k-ε* model. Following refs. [8-10] the general form of elliptic differential equations governing two-dimensional, turbulent, steady, incompressible, isothermal, two-phase flow through 90° bend shown in fig. 1 is given by,

$$\frac{1}{y^j}\frac{\partial}{\partial y}(\alpha\rho y^j v\,\Phi)+\frac{1}{y^j}\frac{\partial}{\partial\theta}(\alpha\rho v\Phi)$$
$$=\frac{1}{y^j}\frac{\partial}{\partial y}\left(\alpha\,\Gamma_\Phi y^j\frac{\partial\Phi}{\partial y}\right)+\frac{1}{y^j}\frac{\partial}{\partial\theta}\left(\alpha\Gamma_\Phi\frac{\partial\Phi}{y^j\partial\theta}\right)+S_\Phi-S_p^\Phi, \tag{1}$$

where, $j = 1$, $y = r$ for curved duct, while for straight ducts $j = 0$, $\theta = x$. and the S^Φ and $S_p{}^\Phi$ are source terms of gas and dispersed phases respectively, while the effective viscosity, and exchange coefficient, Γ_Φ are summarized in table 1 for the dependent variable Φ. Constants of the two used models are taken as in table 2.

The effective and eddy viscosities are taken and calculated for standard *k- ε* (model-1) and RNG based *k- ε* (model-2) as in refs. [8, 10], respectively as,

Standard k-ε, model

$$\mu_{eff}=\mu+\mu_t,\qquad \mu_t=C_\mu\rho\frac{k^2}{\varepsilon}. \tag{2}$$

RNG based k-ε model

$$\mu_{eff}=\mu\left[1+\sqrt{\frac{C_\mu\rho}{\mu}}\frac{k}{\sqrt{\varepsilon}}\right]^2,\ \mu_t=\mu_{eff}-\mu. \tag{3}$$

The Prandtl number, σ_k and σ_ε are calculated as follows,

$$\left|\frac{\lambda-1.3929}{\lambda_o-1.3929}\right|^{0.6321}\left|\frac{\lambda+2.3929}{\lambda_o+2.3929}\right|^{0.3679}=\frac{\mu}{\mu_{eff}} \tag{4}$$

where, λ is an inverse Prandtl number with λ_o=1.

Table 1
Governing equations of gas phase

Conservation of	Φ	Γ_Φ	S^Φ	S_p^Φ
Continuity	1	0	0	0
Axial momentum	u	μ_{eff}	$\frac{1}{y^j}\frac{\partial(\alpha p)}{\partial\theta}+\frac{\partial}{\partial y}\left(\alpha\mu_t\left(\frac{\partial v}{y^j\partial\theta}-j\frac{u}{y^j}\right)\right)$ $+\frac{1}{y^j}\frac{\partial}{\partial\theta}\left(\alpha\mu_t\left(\frac{\partial u}{y^j\partial\theta}+j\frac{2v}{y^j}\right)\right)$ $+j\left(\frac{\alpha\mu_{eff}}{y^j}\left(2\frac{\partial v}{y^j\partial\theta}-\frac{u}{y^j}\right)-\frac{\alpha\rho uv}{y^j}+\frac{\alpha\mu_t}{y^j}\left(\frac{\partial u}{\partial y}-\frac{u}{y^j}\right)\right)$	$\frac{1}{V_c}\Sigma F_\theta$
Radial momentum	v	μ_{eff}	$-\frac{\partial(\alpha p)}{\partial y}+\frac{1}{y^j}\frac{\partial}{\partial y}\left(\alpha\mu_t y^j\frac{\partial v}{\partial y}\right)+\frac{1}{y^j}\frac{\partial}{\partial y}\alpha\mu_t\left(\frac{\partial v}{xy}-j\frac{u}{y^j}\right)$ $+j\left(\frac{\alpha\rho u^2}{y^j}-\frac{\alpha\mu_{ef}}{y^j}\left(2\frac{\partial u}{y^j\partial\theta}+\frac{v}{y^j}\right)-\alpha\mu_t\frac{v}{y^{2j}}\right)$	$\frac{1}{V_c}\Sigma F_\theta$
Turbulent kinetic energy	k	$\frac{\mu_{eff}}{\sigma_k}$	$\alpha\,(G-\rho\varepsilon)$	S_p^k
Energy dissipation	ε	$\frac{\mu_{eff}}{\sigma_\varepsilon}$	$\alpha\frac{\varepsilon}{k}(C_1\,G-C_2\,\rho\varepsilon-R)$	S_p^ε

Table 2
Constants values of the two used models

Model	C_μ	σ_k	σ_ε	S_p^k	S_p^ε	χ	η_o	R
Standard k-ε model	0.09	1.0	1.3	0.0	0.0	-	-	-
RNG based k-ε model	0.0845	eq.(4)	eq.(4)	eq.(6)	eq.(7)	0.015	4.38	eq. (8)

The turbulent kinetic energy generation term G is evaluated from,

$$G=\mu_t\left(\left(2\frac{1}{y^j}\frac{\partial u}{\partial\theta}+j\frac{v}{y^j}\right)^2+2\left(\frac{\partial v}{\partial y}\right)^2+\left(\frac{1}{y^j}\frac{\partial v}{\partial\theta}+\frac{\partial u}{\partial y}-j\frac{u}{y^j}\right)^2\right). \quad (5)$$

The effect of particulate phase on the turbulent structure can be neglected in standard k-ε model for equilibrium gas-solid flow of high density ratio [8]. While in RNG based k-ε model particulate phase affect the turbulent structure and it can be written as reported in [10] for k and ε equations, respectively, as follow,

$$S_P^k = 2.k\left[\frac{\rho_p}{\tau_p}\right]\left[1-\exp(-B_k\,\frac{\tau_P}{\tau_1})\right]. \quad (6)$$

$$S_P^\varepsilon = 2.\varepsilon\left[\frac{\rho_p}{\tau_p}\right]\left[1-\exp(-B_\varepsilon\,\frac{\tau_P}{\tau_1})\right]. \quad (7)$$

Where B_k, B_ε are constants and taken as 0.09 and 0.4 respectively as in [10]. While $\tau_1 = k/\varepsilon$ and τ_p is the particle relaxation time. The rate of strain R in the ε equation of RNG based k- ε model is expressed as given in [10] by,

$$R = \frac{C_\mu \eta^3((1-\eta/\eta_o)}{1+\chi\eta^3}\varepsilon \quad . \quad (8)$$

$$\mathrm{S} = \sqrt{\mathrm{G}/\mu_\mathrm{t}}, \quad \eta = S\frac{k}{\varepsilon}. \quad (9)$$

2.2. Particle phase modelling

The solid phase is treated by the Lagrangian approach, a few thousands of computational particles 'parcels' were traced through the flowfield in each coupling iteration. After each given time step the new position of the parcels and the new translation and angular velocities are calculated from the equations of motion as in [2, 8] through,

$$\frac{d\vec{X}_p}{dt} = \vec{U}_p, \quad (10)$$

$$m_p\frac{d\vec{U}_p}{dt} = \vec{F}_D + \vec{F}_{SL} + \vec{F}_{LM}. \quad (11)$$

$$I_p\frac{d\vec{\omega}_p}{dt} = \vec{T}. \quad (12)$$

$$\vec{T} = \pi\,\mu\,D_p^3 \quad \left[\frac{1}{2}\nabla\times\vec{U} - \vec{\omega}_p\right], \quad (13)$$

where, $\vec{X}_p$ is the particle position vector, $\vec{U}, \vec{U}_p$ are the gas and particle velocity vectors, $\vec{\omega}_p$ is the particle angular velocity vector, T is the torque acting on the particle, I_p is moment of inertia and m_p is the particle mass, $\vec{F}_D, \vec{F}_{SL}$ and $\vec{F}_{LM}$ are the components of the force arising from drag, shear lift and Magnus lift due to particle rotation, respectively and calculated as depicted in [8, 11] as follows,
The drag force is calculated from:

$$F_D = \frac{3}{4}\,\frac{\rho\ \mathrm{m_p}}{\rho_p\ \mathrm{D_p}}\mathrm{C_D}(\vec{U}-\vec{U}_p)\left|\vec{U}-\vec{U}_p\right|. \quad (14)$$

The shear lift force due to the non-uniform relative velocity over the particle is expressed as reported in refs. [11] as,

$$\vec{F}_{SL} = 1.615.D_p\mu\,\mathrm{Re_s^{0.5}}\,C_{SL}\left[\left(\vec{U}-\vec{U}_p\right)\times\vec{\omega}_f\right], \quad (15)$$

where, $\vec{\omega}_f = 0.5(\nabla\times\vec{U})$ is the fluid rotation, $Re_s = \rho D_p^2\left|\vec{\omega}_f\right|/\mu$ is the particle Reynolds number of the shear flow and the coefficient C_{SL} is given as in [11] by,

$$C_{SL} = (1\text{-}0.3314\gamma^{0.5})e^{-Re_p/10} + 0.3314\gamma^{0.5} \qquad R_{ep} \le 400$$

$$= 0.0524\,(\gamma R_{ep})^{0.5} \qquad R_{ep} > 400, \quad (16)$$

where γ is the correction function proposed by [23] and is defined by the ratio between Re_s and Re_p as,

$$\gamma = \frac{\mathrm{Re}_s}{0.5\,\mathrm{Re}_p}. \quad (17)$$

The Magnus lift due to particle rotation is expressed as in [8] by,

$$\vec{F}_{LM} = \frac{1}{2}\rho\,\vec{\mathrm{V}}_\mathrm{r}^2\,\frac{\pi D_p^2}{4}C_{LM}\,\frac{\vec{\omega}_r\times\vec{V}_r}{\left|\vec{\omega}_r\times\vec{V}_r\right|}, \quad (18)$$

where the quantities $\vec{V}_r = \vec{U}-\vec{U}_p$ and $\vec{\omega}_r = \vec{\omega}_f - \vec{\omega}_p$ are the instantaneous relative linear and angular velocities between local fluid and the particle, respectively. The

Magnus lift coefficient may be expressed as in [8] by,

$$C_{LM} = \frac{D_p|\vec{\omega}_r|}{|\vec{V}_r|} \qquad Re_p \le 1$$

$$= \frac{D_p|\vec{\omega}_r|}{|\vec{V}_r|}(0.178 + 0.822\ \mathrm{Re_p}^{-0.522}) \qquad 1<\mathrm{Re_p}<1000. \quad (19)$$

2.3. Inlet and boundary conditions

At the inlet, the axial velocity profile for gas phase is assumed fully developed turbulent velocity profile, where the radial velocity is assumed to be zero. At outlet, the gradient of flow variables in the flow direction; $\partial\Phi/\partial x = 0$ (Neumann conditions), and the radial velocity v which is set to zero. At the solid wall boundaries, however, u = v = 0.0, no-slip conditions.

$$k_{in} = 0.03U_0^2 \ , \varepsilon_{in} = C\mu\frac{k_{in}^{3/2}}{0.01.D} \quad (20)$$

Because the k and ε equations are not solved at the grid point adjacent to the wall, a modelling scheme is required to simulate the variation of eddy viscosity, μ_t. For this purpose the mixing length approach is adopted where the eddy viscosity is modelled as a function of mixing length as in ref. [13].

$$\mu_t = \rho.\ell_m^2\left[\begin{array}{l} 2\left(\frac{1}{y^j}\frac{\partial u}{\partial\theta} + j\frac{v}{y^j}\right)^2 + 2\left(\frac{\partial v}{\partial y}\right)^2 \\ +\left(\frac{1}{y^j}\frac{\partial v}{\partial\theta} + \frac{\partial u}{\partial y} - j\frac{u}{y^j}\right)^2 \end{array}\right]^{1/2}, \quad (21)$$

where ℓ_m is the mixing length. For smooth walls l_m is calculated from Van Dsiert`s equation, [13] as,

$$\ell_m = Ky_p\,(1- exp\,(-y^+ / A)), \quad (22)$$

where, A is constant which assumes a value of 26 for smooth walls in the equilibrium near wall layer. Also to improve the accuracy of RNG based k-ε the second-order finite difference formula is used to evaluate the velocity gradient at the wall. This can be written as, in [14] as,

$$\left(\frac{\partial u}{\partial y}\right)_w = \frac{-8u_w + 9u_1 - u_2}{3y_w} + O(y_w^2), \quad (23)$$

where, y_w is the thickness of the cell adjacent to the wall, u_w =0.0 for stationary wall and no slip condition, u_1 and u_2 are the velocities at the next two grid points, respectively.

2.4. Particle wall interaction

The condition of rebound is achieved if the particle velocity before collision, w_{p1} is greater than the critical particle velocity, $w_{p,cr}$ as in ref. [15]. The solution of the momentum equations with Coulombs law of friction yields a set of equations for sliding and non-sliding collision process [16,17]. The condition for non-sliding collision is obtained in the form,

$$\left|u_{p1} - \frac{D_p}{2}\vec{\omega}_{p1}\right| \le \frac{7}{2}\mu_0(1+e)v_{p1}$$

Here, the subscript 1 refers to the particle velocity components before impact, μ_o is the static coefficient of friction. The values of restitution and friction coefficients are taken as 0.9 and 0.4, respectively as in ref. [18] for all calculations.

2.5. Solution procedure and convergence

The solution procedure of finite volume descretisation scheme, is solved over the grid cells shown in fig. 1. Pressure-velocity coupling was realised by SIMPLE algorithm [19]. The solution procedure for the fluid and particulate phase is as follows:

1- A converged solution of gas phase is calculated without source term of the dispersed phase and with gas void fraction, α of unity. Convergence solution is accepted at normalized residuals less than 0.002.

2- By numerically integrating the translational and rotational equation of motion for each

parcel in a small time step Δt using fourth order Runge-Kutta, a large number of discrete parcels are traced through the flowfield. The time step is selected to achieve trajectory independent for each run case.

3- The void fraction for dispersed phase, β and for gas phase, α are calculated using trajectory method as [20],

$$\beta = \sum_{traj} \frac{n_k \Delta t_k V_p}{V_c}, \quad \alpha = 1 - \beta . \tag{24}$$

Here, n_k is the number of actual particles in the computational particle (k), V_P is the volume of the particle, V_c is the volume of computational cell and $\sum_{traj}$ means summing over all trajectory passing through the computational cell. The source term of dispersed phase in the gas momentum equation is calculated as in [8] by,

$$S_p = \frac{\beta \rho_p}{m_p n} \sum_{k=1}^{n} (\vec{F}_{D_k} + \vec{F}_{LS_k} + \vec{F}_{LM_k}) , \tag{25}$$

where, n is the number of trajectories passing through the computational cell.

4- The gas flow field is recalculated taking into account the source term and void fractions resulting in step 3

5- Repeat step 2 through 4 until the maximum error in the axial gas velocity between two successive coupled iteration is less than 0.0001 of the inlet mean velocity.

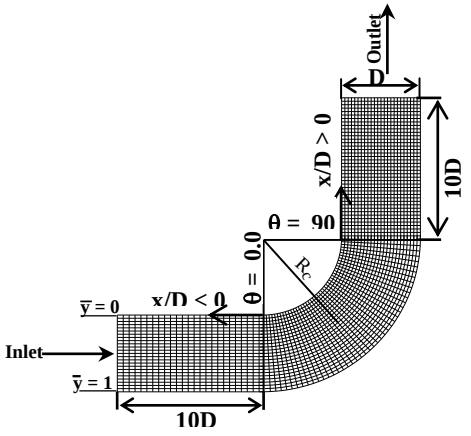

Fig. 1. Duct geometry and computational cell.

2.6. Model verifications

To validate the models used in this study to simulate the flow in a horizontal to horizontal bend, the models have been tested against the results from different sources [5, 6 and 20]. These are presented in figs. 2-3 under the same conditions for gas and solids through the tested duct. It is evident from the figures that there is a reasonable agreement between the present predictions (model-1) and previous data. While in the case of the other one (model-2) a good agreement is obtained.

3. Results and discussions

3.1. Velocity distributions

Figs. 4-7 show the effect of inlet flow velocity U_o, particle diameter (D_p), curvature ratio (δ) and mass loading ratio (Mr) on the normalized axial velocity profiles for gas and particulate phases. From these figures it is easy to conclude generally that, as the flow approaches the bend the maximum value of axial air velocity is shifted towards the inner wall as a result of the favourable pressure gradient and also a deceleration of the flow near the outer wall due to the unfavourable pressure gradient. As the flow progresses further into the bend (θ = 0, 30°) the gas and particulate phases axial velocities increase at the inner duct wall as the particle diameter decreases, and curvature ratio increases. Towards the outer wall of the upstream pipe and bend (x/D = -1, θ = 0, 30 and 60°) the results indicate that the particles have higher velocities (negative slip) than the air velocity. This is can be explained as, the motion of the larger particles is dominated by their inertia and hence they deviate considerably from the gas streamlines within the curved duct. The length of the negative slip velocity region decreases as the flow progresses into the bend. While the solid velocity profiles are found to be considerably flat and is only presented in the central bulk of the flow that correspond to the particle positions after they have rebounded from the outer wall of the duct. Also it is seen that there is a large interphase slip velocity between the gas and particulate phases particularly as the inlet gas

velocity, and particle diameter increase and curvature ratio decreases. This effect is presented for all the stations tested in the present study. This can be attributed to the flatter distribution of axial velocity profiles that appear in the large particle results. In the case of higher values of curvature ratio and particle diameter, a sudden increase in normalized axial particle velocity is seen near the outer wall of the bend. This is may be due to the effect of particles impingement with the bend wall which changes their direction through the bend. Fig. 7 shows that mass loading ratio has an effect on the gas phase through the bend. Further downstream the bend the mass loading ratio has an opposite effect on the gas and particulate phase as a result of the increase of number of particles in the flow.

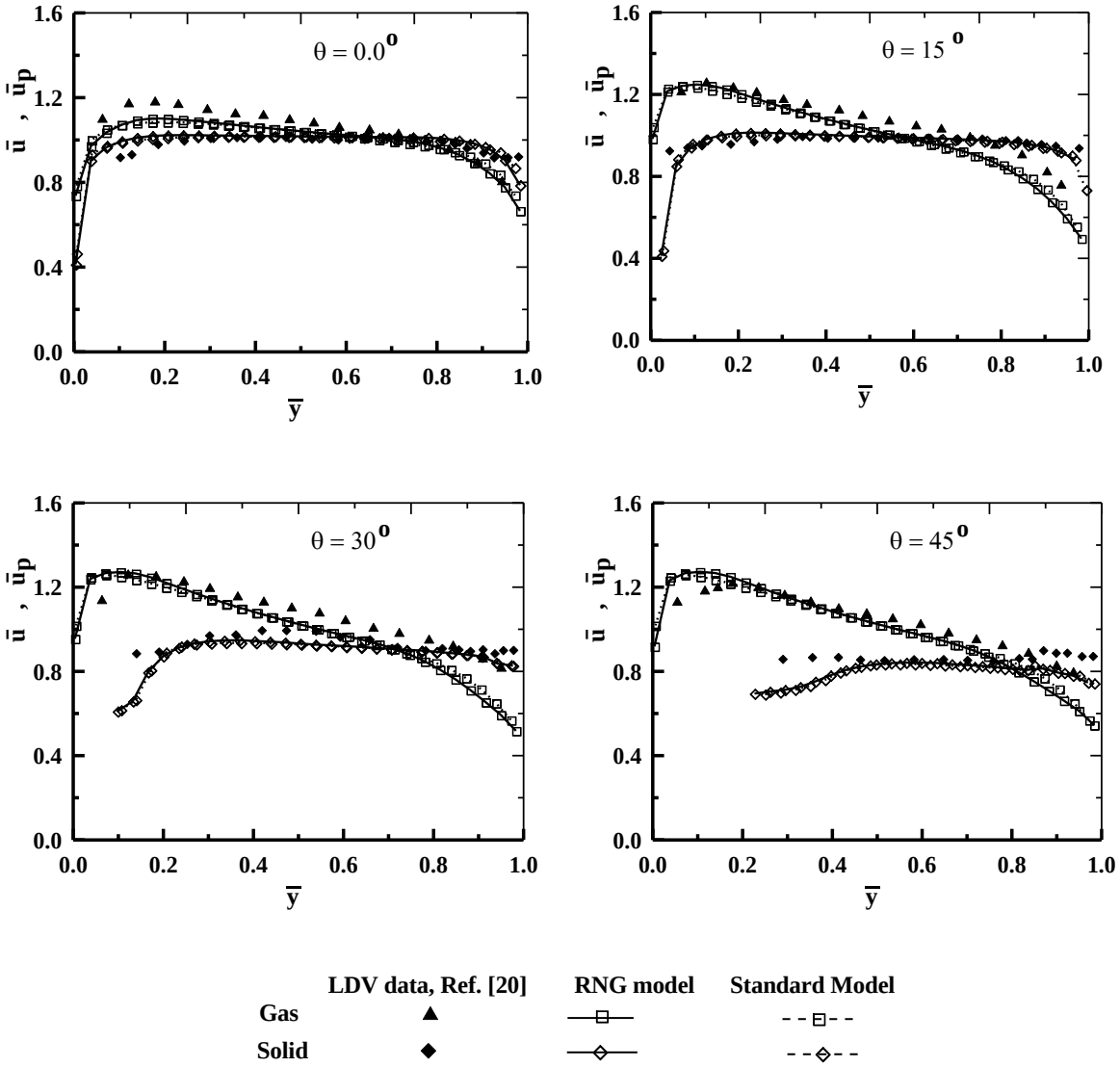

Fig. 2. Comparisons between predicted normalized axial velocity for both phases with LDV measured published data of ref. [20].

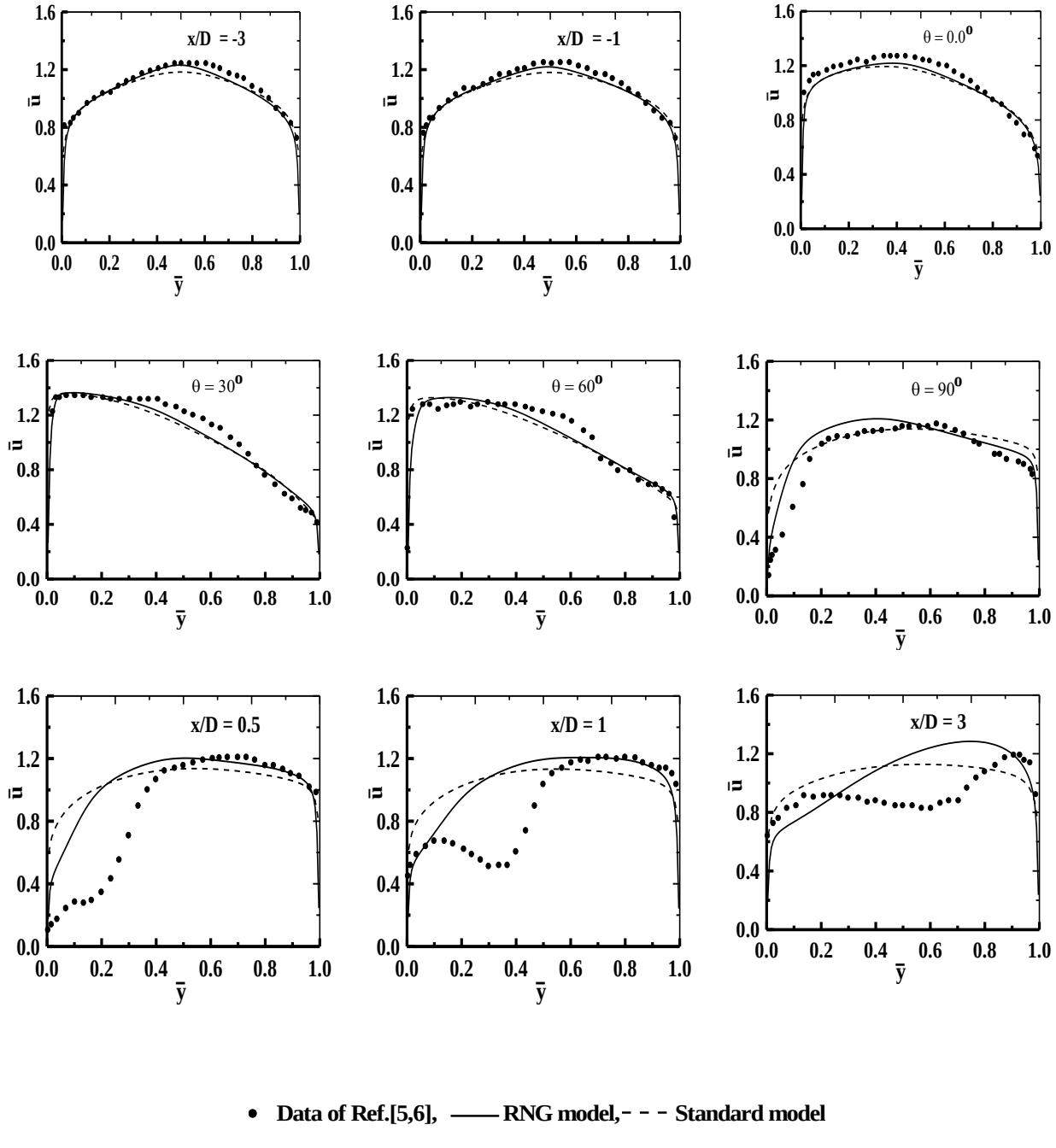

Fig. 3.Comparison between predicted normalized axial gas velocity and published experimental data of refs. [5, 6].

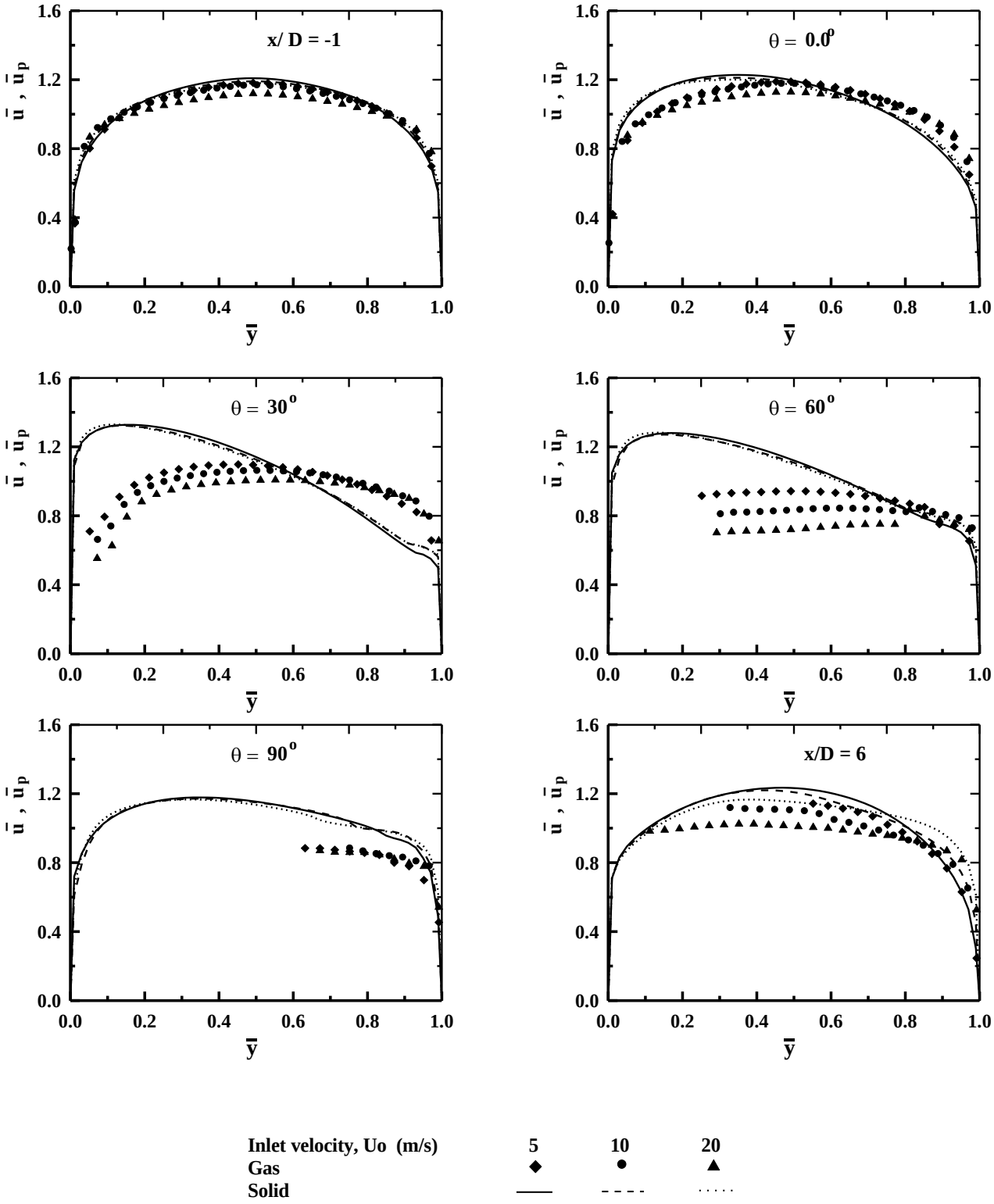

Fig. 4. Effect of inlet flow velocity on the normalized axial velocity for both phases at (Mr = 0.5, δ= 0.33, D_p = 100 μm)

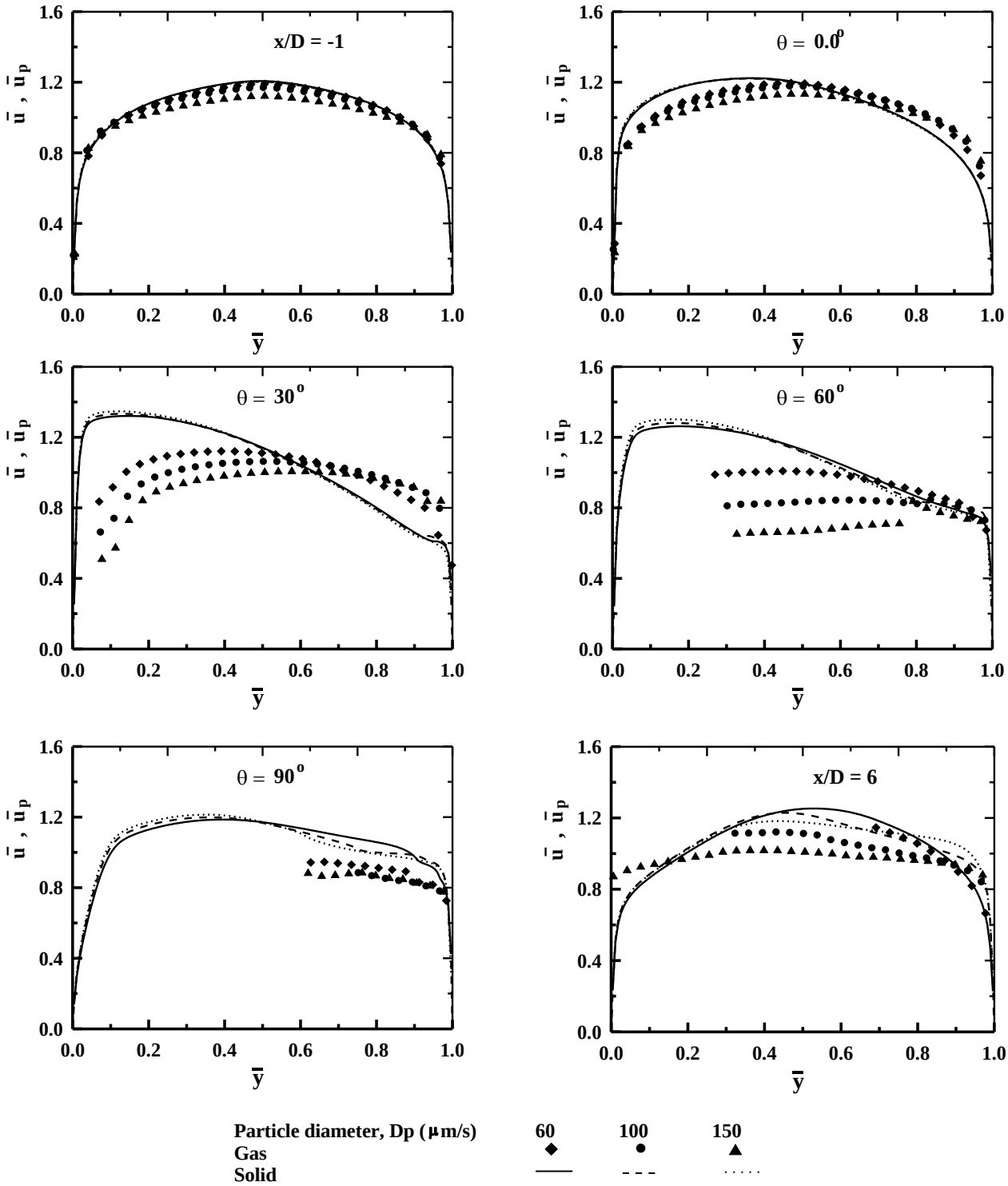

Fig. 5. Effect of particle diameter on the normalized axial velocity for both phases. (U_o= 10 m/sec, δ = 0.33, M_r= 0.5).

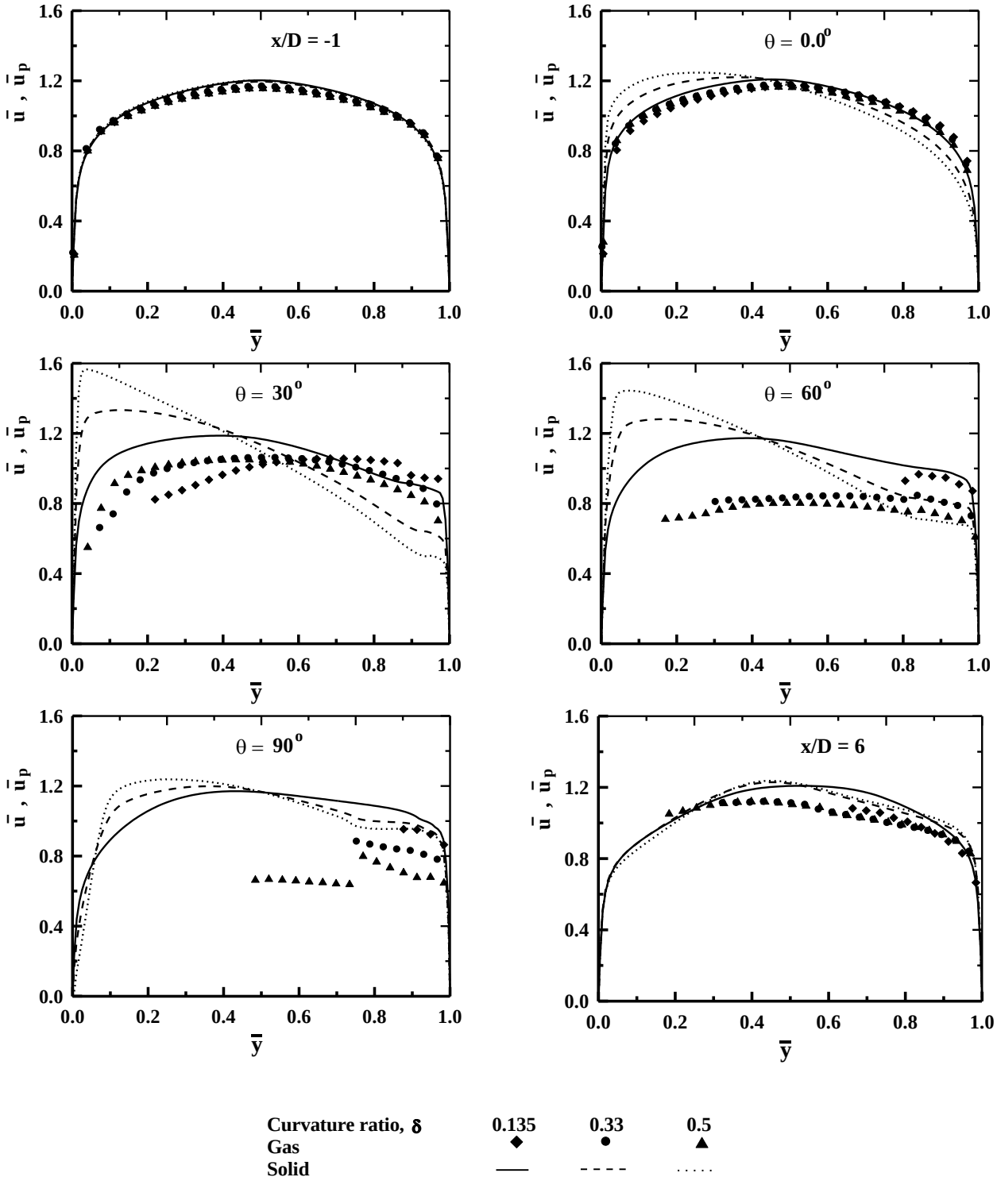

Fig. 6. Effect of curvature ratio on the normalized axial velocity for both phases.
(U_o= 10 m/sec, D_p=100 μm, M_r= 0.5).

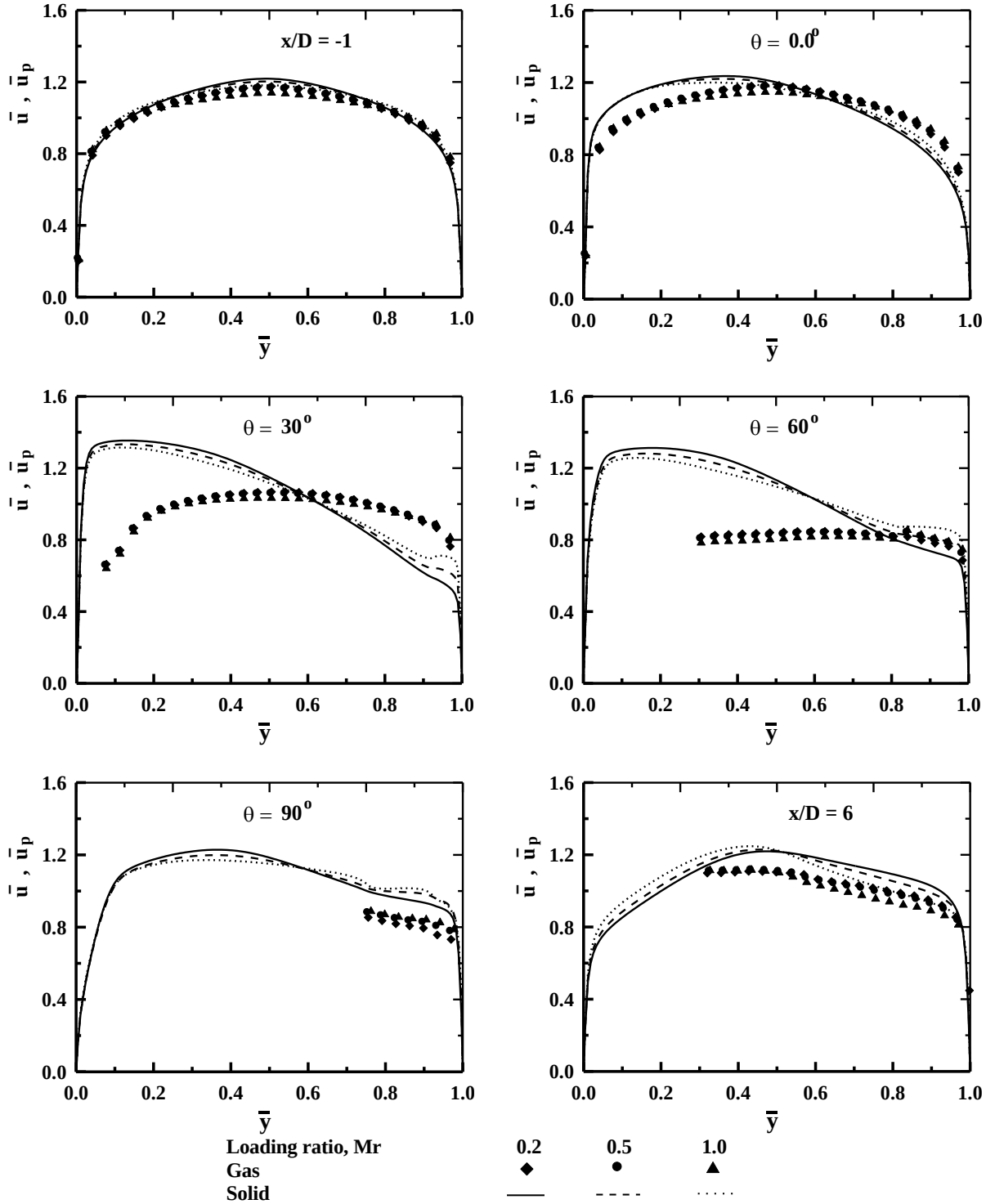

Fig. 7. Effect of loading ratio on the normalized axial velocity for both phases.
(U_o= 10 m/sec, δ= 0.33, D_p = 100 μm).

3.2. Pressure distributions and bend losses

Figs. 8-9 show the effect of inlet flow velocity U_o, particle diameter (D_p), curvature ratio (δ) and mass loading ratio (Mr) on the wall pressure distributions, total pressure loss in the bend and bend loss coefficient. The variations of pressure distributions on the inner and outer wall of the upstream straight duct, bend and downstream the bend are shown in fig. 8. The total pressure loss and accompanied bend loss coefficient are shown in fig. 9. The present results are qualitatively similar to that of [23] and the present calculations revealed that total pressure loss ΔP_b, for gas-solid two-phase flow in 90° bend is greater than the corresponding quantity obtained for gas only (Mr = 0.0). Also the figures indicate that the flow parameters and solid conditions greatly affect the total pressure loss. This may be due to that the total pressure loss is considered as the sum of two quantities namely, the pressure loss due to the gas alone and the other is caused by the solids. The first one is a function of curvature ratio of the bend and Reynolds number, while the second is a function of curvature, solid properties and loading ratio. The models have been tested against the results of other investigators as shown in fig. 10. It is evident from this figure that there is a reasonable agreement between the present predictions of static pressure distributions on the wall and the experimental results of Kim and Patel [23].

3.3. Particles trajectories

It can be seen from figs. 11-13 that very few particles are found in the region near the inner wall of the bend. It can be concluded that particle-wall interaction is a main controlling factor for the outer wall region of the flow. The behaviour of the present results is also in qualitative agreement with the observation of [22]. In addition the results show that only the outer wall is impacted by the particles. From these figures It is also concluded that the particle concentration is further increased near the outer wall and decreased near the inner wall with the increase of Dp. Further progresses of the flow into the bend, a particle free region starts to be identified close to the inner wall. The thickness of this particle free region gradually increases until the bend exit

4. Conclusions

Two particulate turbulence models have been studied to predict the behaviour of turbulent gas-solid flows in bends taking into account the particle wall interaction. The effect of varying the particle diameter, curvature ratio and mass loading ratio on the flow parameters were demonstrated. The second model (RNG) illustrated a good agreement with the experimental data and the numerical results published previously. The particle trajectories were found to be useful tools for explaining the behaviour of gas-solid flow through bends. The present results help to understand the physical phenomena occurring in gas-solid flows in a 90 ° bends. It is concluded that, the total pressure loss for gas-solid two-phase flow in 90° bend is greatly affected by the gas flow and solid parameters.

Nomenclature

D	is the diameter of bend, m
D_p	is the particle diameter, μm
e	is the restitution coefficient,
Mr	is the Mass loading ratio, (m'_p / m'_g)
P	is the pressure, N/m^2
R_C	is the mean bend radius of curvature, m
t	is the Time, sec
u, v	is the mean axial and radial velocities, m/s
$\overline{U}, \overline{U}_p$	is the normalizing mean axial gas and particle velocities
u_{p1}, v_{p1}	is the mean axial and radial particle velocities before impact, m/s
u_{p2}, v_{p2}	is the mean axial and radial particle velocities after rebound, m/s
U_o	is the mean-bulk longitudinal velocity, m/s
y	is the normal coordinate measured from the inner wall, m, and
x	is the axial coordinates along the straight ducts.

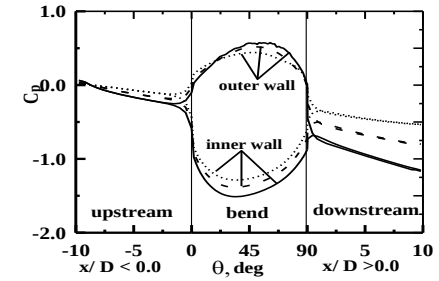

a. Effect of particle diameter

Dp = 60, Dp = 100 , Dp = 150 μm

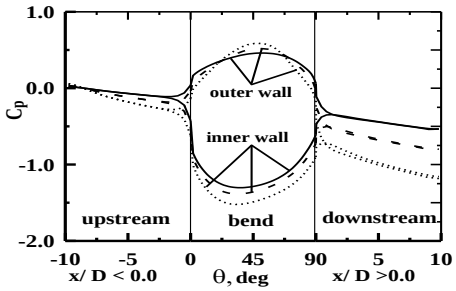

b. Effect of mass loading ratio

Mr = 0.2, Mr = 0.5, Mr = 1.0

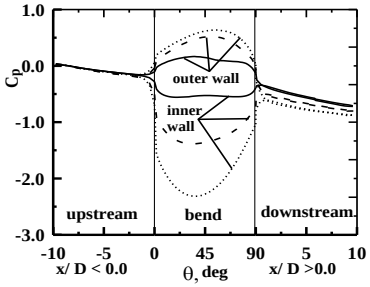

c. Effect curvature ratio

δ = 0.135 , δ = 0.33 , δ = 0.5

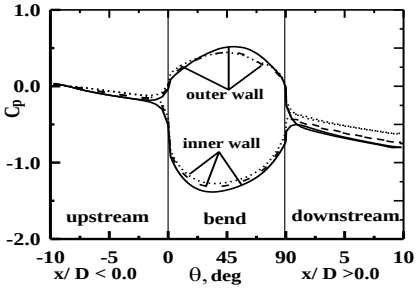

d. Effect of inlet gas velocity

Uo = 5, Uo = 10, Uo = 20 m/sec

Fig. 8. Wall pressure distribution along upstream duct, 90 ° bend and downstream duct.

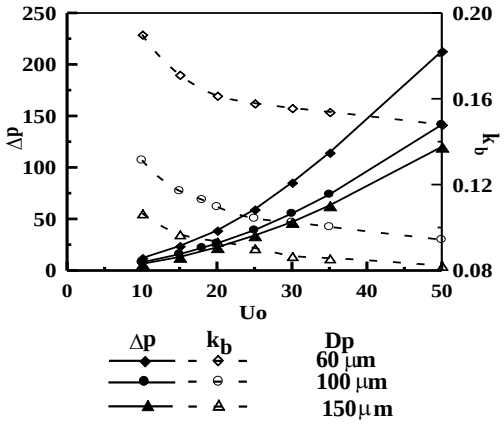

a- Effect of particle diameter

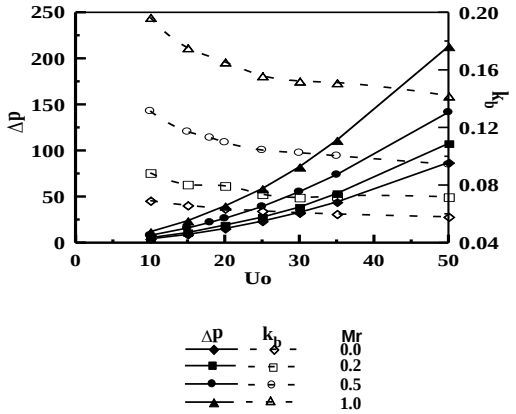

b. Effect of mass loading ratio

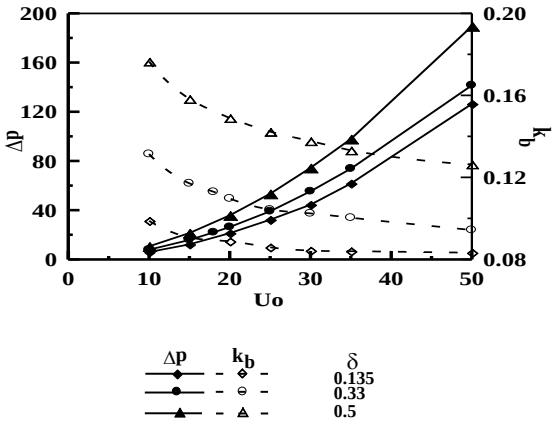

c. Effect curvature ratio

Fig. 9. Bend pressure drop, Δp_b in pa and bend loss coefficient, k_b.

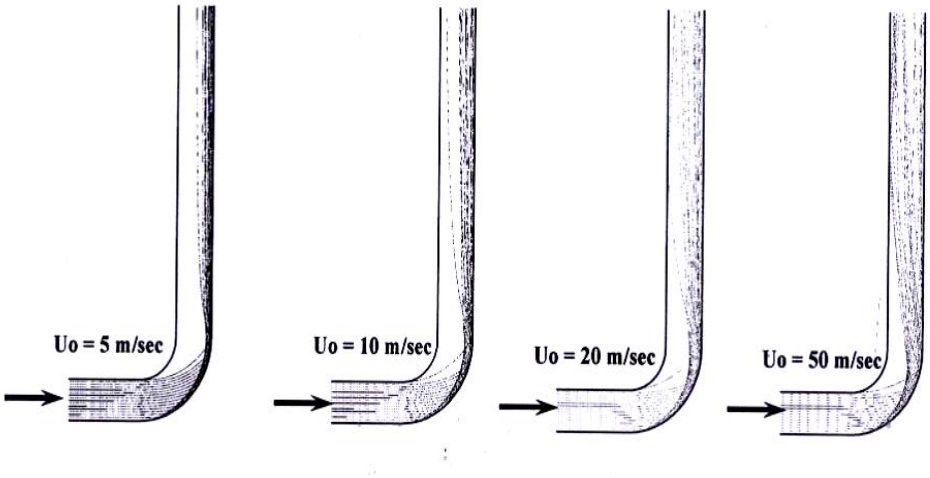

Fig.11. Effect of inlet velocity on the particles trajectories, (δ= 0.33, D_p= 100 μm).

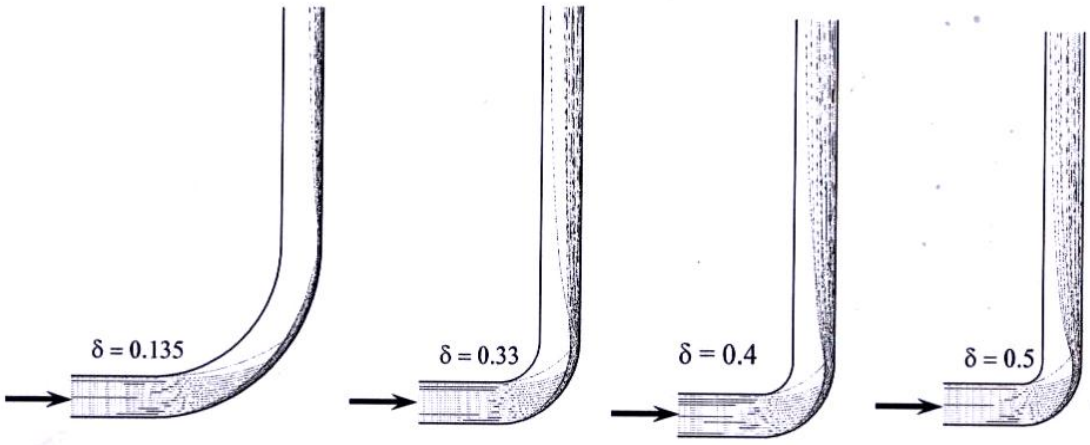

Fig. 12. Effect of curvature ratio on the particles trajectories, (U_o=10m/sec, D_p=100μm).

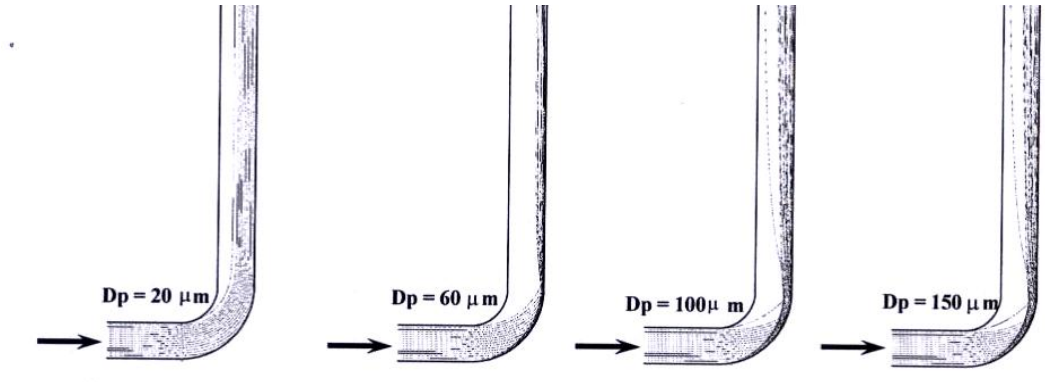

Fig. 13. Effect of particle diameter on the particles trajectories, (U_o=10 m/sec , δ= 0.33).

Greek symbols

α is the gas phase void fraction,
β is the solid phase void fraction,
δ is the curvature ratio ($D/2.R_c$),
Φ is the general dependent variable,
μ is the viscosity, $N.s/m^2$
θ is the axial coordinate along the bend, degree
ρ is the density, Kg/m^3
$\omega_{p,i}$ is the particle angular velocity before impact and after rebound, x rad/s
ω_r is the Relative angular velocity vector, rad/s.

Subscripts

b bend
p Particle

References

[1] Yilmaz Ali and E.K. Levy, "Formation and Dispersion of Ropes in Pneumatic Conveying", Powder Tech., Vol. 114, pp. 168-185 (2001).

[2] N. Huber, M. Sommerfeld, "Modelling and Numerical Calculation of Dilute-Phase Pneumatic Conveying In Pipe Systems", Powder Tech., Vol. 99, pp. 90-101 (1998).

[3] H. Akilli, E.K. Levy, B. Sahin, "Gas-Solid Flow Behavior in a Horizontal Pipe After a 90° Vertical-to-Horizontal Elbow", Powder Tech., Vol. 116, pp. 43-52 (2001).

[4] Bilirgen Harun, K. Levy Edward, "Mixing and Dispersion of Particle ropes in Lean Phase Pneumatic Conveying", Powder Tech., Vol. 119, 2001, pp. 134-152.

[5] B. Kuan, Yang William, Solnordal Chris, "CFD Simulation and Experimental Validation of Dilute Particulate Turbulent Flow in 90° Duct Bend", 3rd Int. Conf. on CFD in the Minerals and process Ind. (2003).

[6] B.T. Kuan, "CFD Simulation of Dilute Gas-Solid Two-Phase Flows with Different Solid Size Distribution in a Curved 90° Duct Bend", ANZIAM J., Vol. 46 (E), pp. C744-C763 (2005).

[7] M. Hidayat, A. Rasmuson, "Some Aspects on Gas-Solid Flow in U-Bend: Numerical Investigation", Powder Tech., Vol. 153, pp. 1-12 (2005).

[8] C.K.K, Lun Liu H.S., "Numerical Simulation of Dilute Turbulent Gas-Solid Flows in Horizontal Channels", Int. J. Multiphase Flow, Vol. 23, pp. 575-605 (1997).

[9] L. Michael Santi, "Turbulent Flow Field Prediction in Sharply Curved Turn-Around Ducts", NASA Contractor Rept. 3990 (1986).

[10] A. Eghlimi, A. Kouzoubov, C.A.J. Fletcher "A new RNG-Based Two-Equation Model for Predicting Turbulent Gas-Particle Flows", Int. Conf. on CFD in Mineral and Metal Processing and Power Generation (1997).

[11] R. Mei, "An Approximate Expression for the Shear Lift Force on a Spherical Particle at Finite Reynolds Number", Int. J. Multiphase flow, Vol. 18, pp. 145-147 (1992).

[12] D.D. Kladas and D.P. Deorgiou, "A Relative Examination of CD - Re Relationships used in Particle Trajectory Calculations ", ASME J. of Fluids Engineering, Vol. 115, pp. 162-165 (1993).

[13] FLUENT Theory Manual, "Turbulence Modelling, Section 10-7 [online]", Available at ***http://www.shef.ac.uk/mecheng/staff/xyl/fidap/help/theory/th10_03-08.htm#th_1007*** [Last accessed 21 January (2006)].

[14] J.D., Jr. Anderson "Computational Fluid Dynamics", McGraw Hill Inc. (1995).

[15] E. Heinl, M. Bohent "Calculation of Particle-Wall Adhesion in Horizontal Gas-Solid Flow Using CFD", Powder Tech., Vol. 159, pp. 95-104 (2005).

[16] Y. Tsuji, Y. Morikawa T. Tanaka, N. Nakatsukasa and M. Nakatani, "Numerical Simulation of Gas-Solid two-Phase flow in Two-Dimension Horizontal Channel", Int. J. Multiphase flow, Vol. 13, pp. 671-684 (1987).

[17] M. Sommerfeld "Modelling of Particle-wall Collisions in confined Gas-Particle Flows", Int. J. Multiphase Flow, Vol. 183, pp. 905-926 (1992).

[18] M. Sommerfeld, N. Huber, "Experimental Analysis and Modelling of Particle-Wall

Collisions", Int. J. Multiphase flow, Vol. 25, pp. 1457-1489 (1999).
[19] S.V. Patankar, "Numerical Heat Transfer and Fluid Flow", McGraw-Hill, New York, U.S.A. (1983).
[20] C. Crowe, M. Sommerfeld and Y. Tsuji, "Multiphase flow with Droplets and Particles", CRC Press, Florida, U.S.A. (1998).
[21] Y. Kliafas and M. Holt, "LDV Measurements of a Turbulent Air-Solid Two-Phase Flow in a 90° Bend", Experiment in Fluids, Vol. 5, pp 73-85 (1987).
[22] S. Naik and I.G. Bryden, "Prediction of Turbulent Gas-Solids Flow in Curved Ducts Using the Eulerian-Lagrangian Method", Int. J. Numerical. Methods Fluids, Vol. 31, pp 579-600 (1999).
[23] Wu J. Kim and V.C. Patel, "Origin and Decay Longitudinal Vortices in Developing Flow in a Curved Rectangular Duct", Transactions of the AMSE, J. fluid Engineering, Vol. 116, pp 45-52 (1994).

Received April 18, 2006
Accepted June 7, 2006